Structural and optical characterization of new lanthanide-doped perovskites.

Garoé Medina-Aguilar[a], Fernando Déniz-Correa[a], Antonio D. Lozano-Gorrín[b], Víctor Lavín[c]

[a]Master in Molecular Nanoscience and Nanotechnology, Universidad de La Laguna
[b] Departamento de Química, Universidad de La Laguna
[c] Departamento de Física, Universidad de La Laguna

ARTICLE INFO

Keywords:
Perovskite-type
Oxides
Erbium
Neodymium
Structural
Characterization
Optical properties

ABSTRACT

Perovskites $SrMoO_3$ doped with Er^{3+} and Nd^{3+} in a range of concentrations from 0.2 to 8 %mol have been studied, by X-ray diffraction, scanning electron microscopy and optical spectroscopy. The structural characterization shows tetragonal symmetry and $I_{41/a}$ (nº 88) as space group. Ultraviolet- Visible- Near Infrared (UV-Vis-NIR) photoluminescence properties have been studied, obtaining that the materials are optically active in the optical due the lanthanide ions. The Er^{3+} doped perovskites exhibit a strong green upconverted emission that can be seen with the naked eye when the sample is excited at 795 nm. This green emission has been studied at different Er^{3+} concentrations and is associated with upconversion processes involving two NIR photons. For the Nd^{3+} doped perovskites a study of the luminescence decay curves is done

1 Introduction

In the recent years, perovskite oxides with general formula ABO_3 are being widely studied due to their incredible properties[1–4], which make them suitable for a wide range of applications such as catalysis[5] , high temperature superconductivity[6], ferroelectricity[7], solid oxide fuel cells(SOFCs)[8] etc. Among the perovskites, $SrMoO_3$ was selected as a general matrix because of its cubic symmetry. Nowadays materials based on $SrMoO_3$ are being researched as promising anode in SOFCs[8–10].

The lanthanide doped perovskites are taking special relevance[11–13], among all trivalent lanthanides (Ln^{3+}), Er^{3+} and Nd^{3+} stand out due to their well-defined peaks, an incredible photostability and long excited states lifetimes[14,15]. All these characteristics make these doped materials of interest for luminescence applications, for example in laser materials[16], optoelectronic and temperature sensors[17]. One of the most important processes that occurs to these lanthanides is the IR-to-visible energy upconversion (UC)[18–21]. This process was discovered in the 1960s by Auzel[22], who described it as a process in which two or more photons of lower energy excitation light, commonly NIR, were converted into photons of higher energy emission light, visible and ultraviolet, by a non-linear anti-Stoke process. This mechanism is different from other optical processes which also use two or more photons of lower energy to produce higher energy emissions such as multiphoton[23], fluorescence[24] or second harmonic generation[25,26]. The difference between these processes and UC is the involvement of intermediate electronic states in the system, the UC process is mediated by electronic states, while in the others a real electronic state does not take part. Because of this difference, the processes based on the simultaneous interaction of two or more photons requires 5 to 10 orders of magnitude higher excitation powers.[27] In order to generate the UC, at least one real metastable states must exist, the lower energy state is normally in the NIR range and acts as an energy storage, then the higher state normally in the Vis range is the responsible of the emission of the upconverted energy photons. The first state must have a long lifetime, making it able to accumulate transient population, which increase the probability of interaction with other photons[28].

There are different UC mechanisms well stablished[29–31]. The majority involves the absorption and non-radiative energy transfer steps. In figure 1 the most important UC processes are schemed. Excited state absorption (ESA) is a single ion mechanism where, the ion absorbs two photons in the same laser pulse, one gets to the intermediate state by ground state absorption (GSA) and the second to a higher energy state. The other process is referred to energy transfer upconversion (ETU), in this mechanism two ions are excited into the intermediate levels via GSA , then by a non-radiative energy transfer between the two ions, one is promoted to a higher excited state, while the other simultaneously relaxes to the ground state. In overall in both processes, two excitation photons are converted into one emitted of higher energy[32].

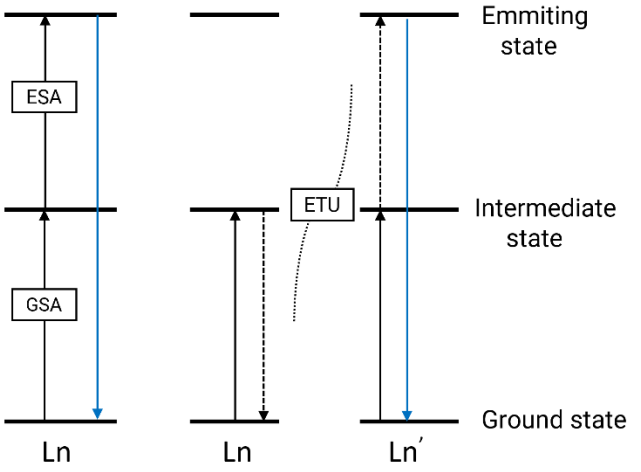

Figure 1. Schematic representation of the most important UC mechanism: Ground state absorption (GSA), excited-state absorption (ESA) and energy transfer upconversion (ETU). Dotted lines represent nonradiative energy transfer processes, downward solid lines indicate radiative transitions.

The lanthanide trivalent (Ln^{3+}) ions are interesting for the upconversion processes because they commonly have more than one metastable level. This is because the optical active 4f electrons are shielded from the environment by outer electrons such us 5s and 5p electrons, so they have small coupling electron-phonon strength. The luminescence processes are more competitive, which make their excited states lifetimes in the order of µs or more[32].

This work presents, for the first time, the synthesis of Er^{3+} and Nd^{3+} $SrMoO_3$ doped perovskites using the ceramic method, as well as the study of the structure by XRD and SEM, as well as the absorption and Stokes and upconverted luminescence properties. The present study compares the luminescence properties as a function of the lanthanide concentration, which act as the optical active ion. The purpose of this research is to characterize these new materials and discuss the possible applications they may have.

2 Experimental methodology

Perovskites with composition $Ln_xSr_{1-x}MoO3$ (Ln= Er or Nd // x= 0,01~0,4) were synthetised by using the ceramic method. The precursor was obtained from mixing erbium oxide (Sigma Aldrich 99.99 %), molybdenum oxide (Sigma Aldrich 99%) and strontium carbonate (Sigma Aldrich 99%) in a planetary ball milling 20 minutes at 600 r.p.m. Then, the precursor obtained was heated at 800 ºC for 12 h, cooled down to room temperature, milled manually in a mortar and heated on a second heat treatment at 1150 ºC for 24 h. The object in these thermal treatments is to achieve the perovskite $SrMoO_3$ structure.[8] The X-Ray powder diffraction of the perovskites was carried out by using a diffractometer (PANalytical X´Pert Pro) with CuKα1 radiation (λ=1,5406 Å) in the range of º2θ from 10 to 80. The scanning electron microscopy images (ZEISS EVO 15 SEM) were measured with 2 nm resolution with a coupled energy dispersive X ray analyser (EDX) (Oxford X-MAX of 50 mm^2). Due the non-conductive and powder nature of the compounds, the samples were prepared with a carbon coating in order to achieve the image[33].

Absorption spectrum was measured on a UV-Vis spectrophotometer (Agilent technologies Cary 5000) by using a diffuse reflectance configuration. The UV-Vis excitation and emission spectra were recorded on a photoluminescence spectrometer (FLS 1000 Edinburgh Instruments) exciting with a 450W Xe arc lamp. The NIR emission spectra were measured by exciting the perovskites with a Ti: Sapphire tuneable laser system, (3900S Spectra Physics) pumped by a 15W 532 mm laser (Spectra Physics Millenia Prime), adjusted at different wavelength depending on the lanthanide. The luminescence was acquired using a spectrometer (Andor Shamrock 500) coupled to a visible and InGaAs CCD cameras. The study of the lifetime of the excited states were done exciting the perovskites with a 10 ns pulsed optical parametric oscillator (OPO EKSPLA/NT342/3/UVE) with a photomultiplier (Hamamatsu R928) as a detector through a single grating monochromator (Jobin-Yvon Triax 180) connected to a digital oscilloscope (LeCroy WS424).

3 Results

3.1 Structure

3.1.1 X-ray Diffraction (XRD)

X-ray patterns of the samples are presented in figure 2. The patterns reveal well defined Bragg positions that were indexed in the structure that exhibit tetragonal symmetry with the space group $I_{41/a}$ No. 88 Z=8.Crystal structure parameters have been obtained after fitting the patterns of each perovskite by the Rietvelt method[34] (see figure 3) using the FULLPROF program.[35,36] The parameters of fitting and reliability factors are shown in table 1.

Table 1. Cell parameters and reliability factors resulted from fitting XRD pattern of the perovskites.

Cell parameters and reliability factors								
Perovskite	a (Å)	b (Å)	c (Å)	V (Å^3)	χ^2	R_p	R_{wp}	R_{exp}
$Nd_{0,2}Sr_{0,8}MoO_3$	5,38	5,38	11,98	347,4	42,7	7,11	13,2	2,02
$Nd_{0,01}Sr_{0,99}MoO_3$	5,40	5,40	12,02	350,0	42,4	7,44	12,5	1,92
$Er_{0,1}Sr_{0,9}MoO_3$	5,39	5,39	12,00	348,6	35,0	6,92	11,9	2,01
$Er_{0,01}Sr_{0,99}MoO_3$	5,40	5,40	12,03	350,3	30,2	6,33	10,5	1,90

Table 1 shows the cell parameters and the reliability factors of some of the studied perovskites, those with high concentration of lanthanide are not shown since their agreement factors were not that good. The reliability factors in general, tends to be low, indicating that a good mathematical treatment was done. Looking at the X-ray patterns (see figure 2) all of them look very similar, and they exhibit the same peaks in almost all °2Θ range; When concentration of lanthanide increases some peaks appears: one around 30°, and the other around 47°. The appearance of these peaks may imply that the perovskite

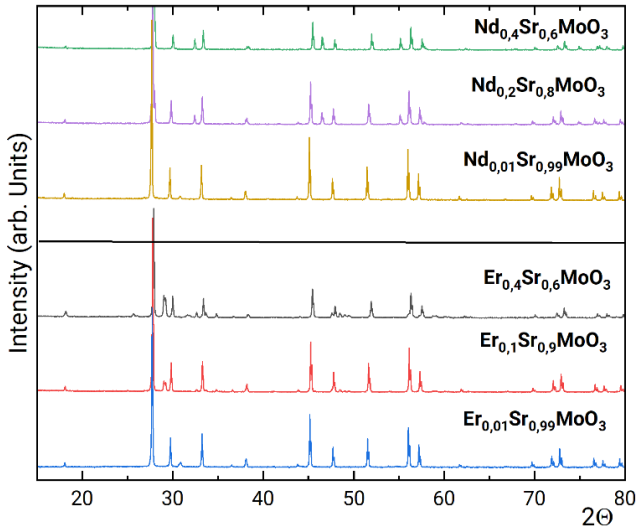

Figure 2. X-Ray diffraction patterns of the different perovskites, on top Nd^{3+} perovskites, at the bottom Er^{3+}Perovskites. Important to note that some diffractograms are moved in order to achieve a better comparison between them.

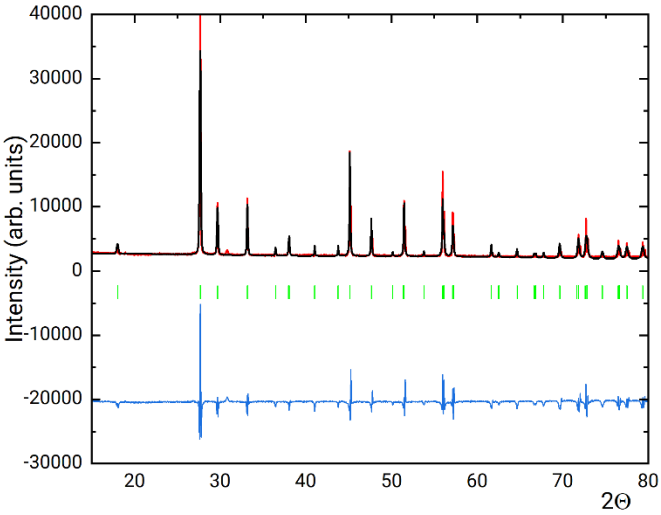

Figure 3. X-ray diffraction pattern with Rietvelt treatment of $Nd_{0,01}Sr_{0,99}MoO_3$. The experimental pattern is observed in red; the calculated pattern is observed in black, the difference between the experimental and the calculated is observed in blue and the Bragg positions as the vertical green lines.

structure is undergoing a symmetry change. The $SrMoO_3$ structure was reported as cubic perovskite[8,37], the inclusion of Ln^{3+} generates a distortion in the cubic structure because they are placed in the position of the Sr^{2+}, this is evidenced by the reduction to tetragonal symmetry that all perovskites present, an increase in lanthanide concentration may cause an even greater decrease in symmetry.

3.1.2 Scanning electron microscopy (SEM)

SEM images are presented in figure 4, where the structure at microscale is observed. The distribution of the elements is presented in figure 4, where SEM images are combined with X-ray diffraction (EDX)[38].

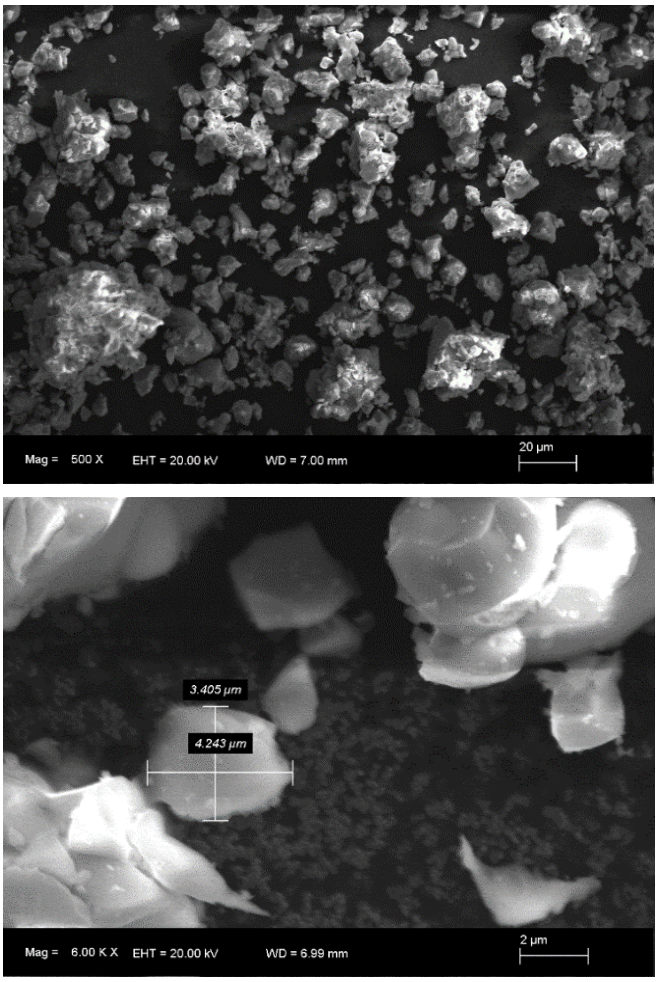

Figure 4. SEM images of the perovskites

In figure 4 the SEM images show the nanocrystalline powder obtained, in which the compound is seen as agglomerated flakes of different shapes and sizes from 10 to 20 µm. In addition, the magnetization of the microscope is shown in both pictures. By observing the bottom image (zoomed one) one can get an approximation value for the grain size, around 4.3 µm in the case shown in figure 4, this value of the grain size is comparable to other studies[39].

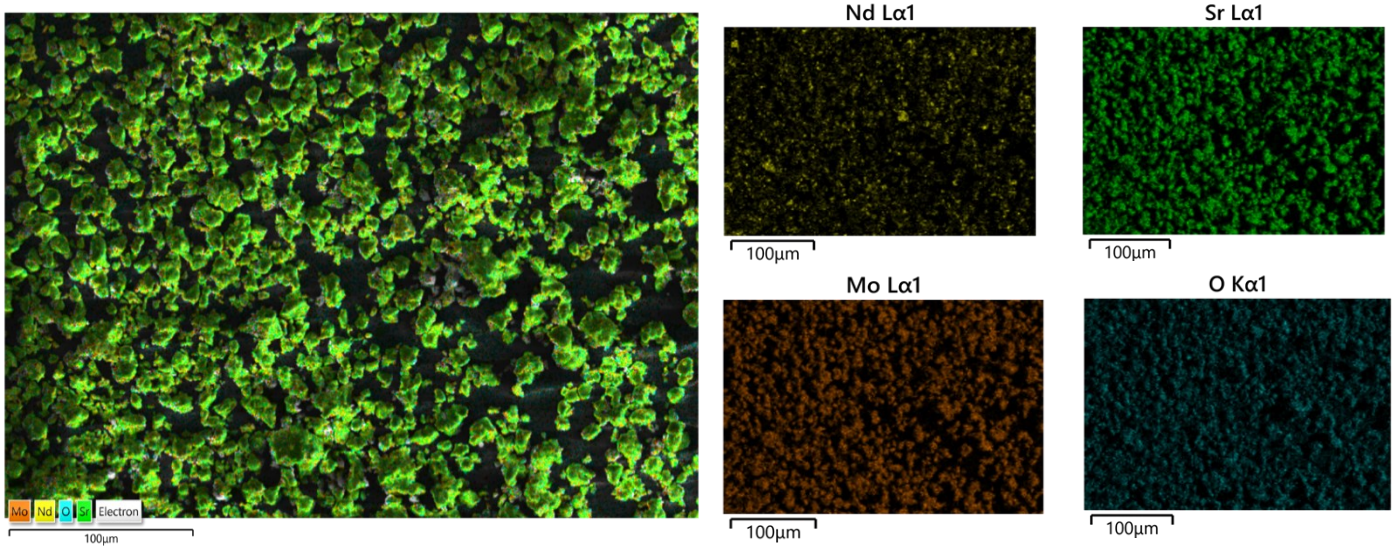

Figure 5. EDX images of the distributions of all the elements, left image shows the complete distribution and the right images show the distribution of every element.

Figure 5 shows that all the elements are homogeneously distributed in the material, indicating that the structure is well defined and the lanthanide, Nd^{3+} in this case, appears to be incorporated in the crystalline structure.

3.2 Photophysical properties

3.2.1 Absorption and luminescence properties

The first step in order to study the optical properties of the Ln-doped perovskites was to analyse the absorption spectra, using an integrating sphere, in order to take absolute values. A total of nine transition bands have been observed for the erbium perovskite, all starting from the $^4I_{15/2}$ ground state (See figure 6).

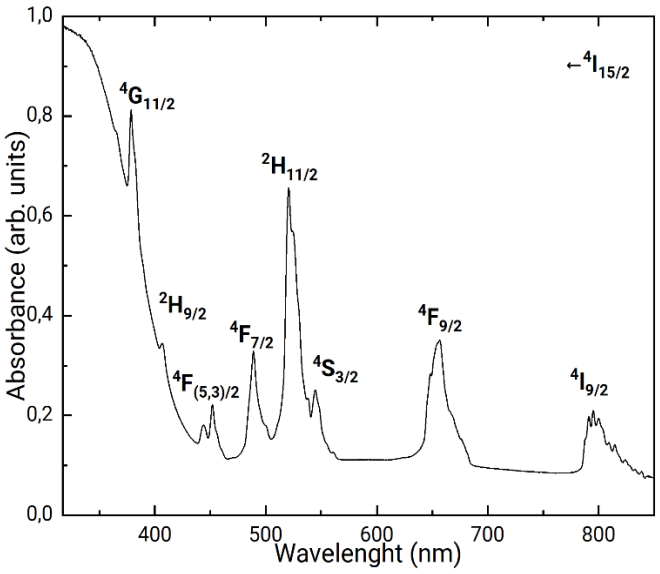

Figure 6. Absorption spectra of $Er_{0,4}Sr_{0,6}MoO_3$ perovskite in the range from 310-880 nm with the transitions from the ground state $^4I_{15/2}$.

For the Er^{3+}-doped perovskite, the transition with the highest absorbance is $^4I_{15/2} \rightarrow {}^4G_{11/2}$ located at 378 nm, and $^4I_{15/2} \rightarrow {}^2H_{11/2}$. This happens because of the hypersensitive nature of these transitions[40].

The emission spectra of the Er^{3+} perovskites are shown in figure 7. We can observe the characteristic green bands of Er^{3+} which corresponds to $(^2H_{11/2}, {}^4S_{3/2}) \rightarrow {}^4I_{15/2}$ transitions with the highest intensities, really close, but with less intensity the red emission corresponding to $^4F_{9/2} \rightarrow {}^4I_{15/2}$ transition. In the NIR range at around 850 nm, corresponding to the $^4S_{3/2} \rightarrow {}^4I_{13/2}$ transition is also obtained. These peaks have also been found in other works when Er^{3+} ions are incorporated into a perovskite structure[41].

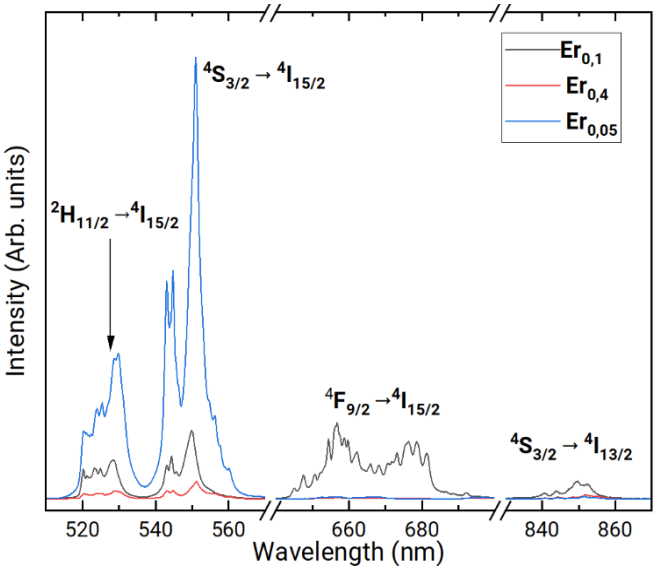

Figure 7. Emission Spectra of different Er^{3+} doped perovskites obtained exciting the $^4I_{15/2} \rightarrow {}^4G11_{/2}$ absorption band under 378nm Xe lamp excitation.

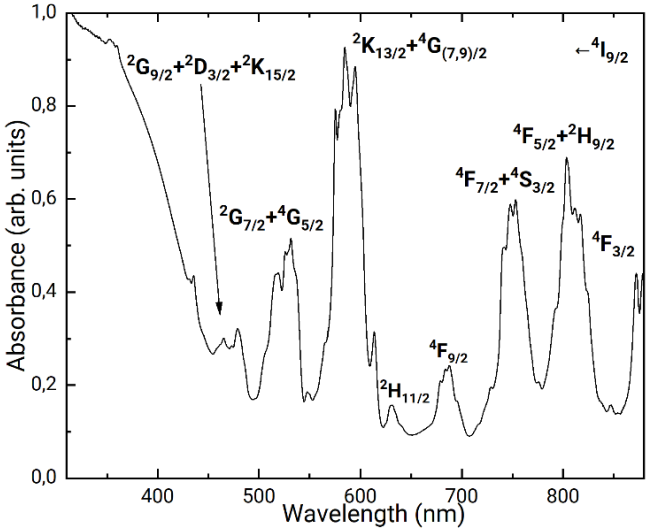

Figure 8. Absorption spectra of $Nd_{0,4}Sr_{0,6}MoO_3$ perovskite in the range from 310-880 nm with the transitions from the ground state $^4I_{9/2}$.

Table 2.Transition states and peaks position for absorbance spectra's

Erbium Perovskites				Nedodymium perovskites			
Transition		Peaks Position		Transition		Peaks Position	
Ground State	Excited State	$Er_{0,4}Sr_{0,6}MoO_3$		Ground State	Excited State	$Nd_{0,4}Sr_{0,6}MoO_3$	
		±0,5nm	10^3cm^{-1}			±0,5nm	10^3cm^{-1}
$^4I_{15/2}$	$^4I_{9/2}$	795,0	12,58	$^4I_{9/2}$	$^4F_{3/2}$	872,5	11,46
	$^4F_{9/2}$	656,5	15,23		$^4F_{5/2}+^2H_{9/2}$	803,5	12,45
	$^4S_{3/2}$	544,5	18,37		$^4F_{7/2}+^2S_{3/2}$	753,0	13,28
	$^2H_{11/2}$	520,5	19,21		$^4F_{9/2}$	687,5	14,55
	$^4F_{7/2}$	489,0	20,45		$^2H_{11/2}$	631,0	15,85
	$^4F_{(5,3)/2}$	452,0	22,12		$^2K_{13/2}+^4G_{(7,9)/2}$	584,5	17,11
	$^2H_{9/2}$	407,0	24,57		$^2G_{7/2}+^4G_{5/2}$	531,5	18,81
	$^4G_{11/2}$	378,5	26,42		$^2G_{9/2}+^2D_{3/2}+^2K_{15/2}$	479,0	20,88

In the case of neodymium, a total of 15 transitions bands have been observed from the $^4I_{9/2}$ ground state (See figure 8). The transitions with the highest absorbance for the Nd^{3+} are $^4I_{9/2} \rightarrow (^2K_{13/2}+^4G_{(7,9)/2})$ where the Nd^{3+} gain access to a triplet excited state.

All these transitions are electrically dipolar in nature forced by the interaction of the 4f electrons of the lanthanide and the valence electrons of the closest ligands, the transitions were assigned using the well-known Dieke's Diagram.[42] All peaks for both perovskites with their wavelengths and energies are listed in table 2. The sharp peaks profile obtained in both spectra confirm that the Er^{3+}/Nd^{3+} ions are incorporated in the crystalline structure of the perovskite.

The dependence of the luminescence and the Er^{3+} concentration is clearly seemed in the mentioned transitions, when the concentration of Er^{3+} decreases, the intensity tends to higher values. This can be explained by different cross-relaxation energy transfer processes involving the ground state and the emitting levels.

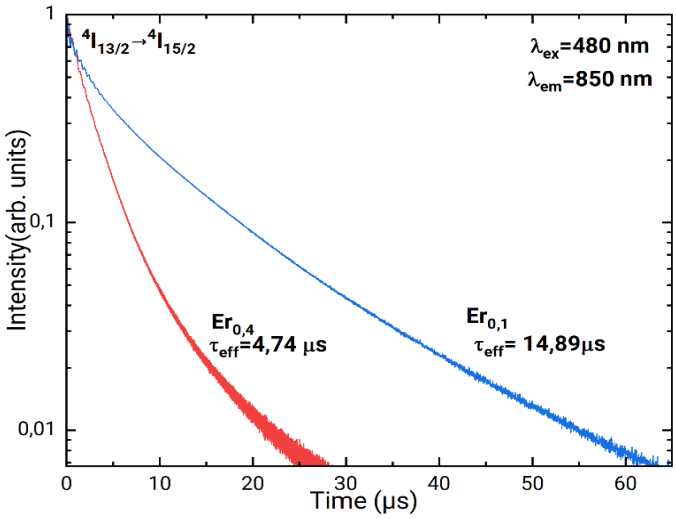

Figure 9. Luminescence decay curves of NIR emissions of different Er^{3+} doped perovskites

In order to check the energy transfer channels, the lifetime of some excited states was measured, for the Er^{3+} doped perovskites (See figure 9), the relaxation observed was the $^4I_{13/2} \rightarrow {}^4I_{15/2}$, exciting wavelength was set at 480 nm and the emission was observed at 850 nm wavelength. For low concentration of optically active ions, it is expected that the interactions between them are negligible, so the luminescence decay is expected to be exponential. Nevertheless, at higher concentrations these active ions are closer to each other, and the energy transfer processes become more efficient, and therefore non-negligible, leading to a non-exponential decay[43,44].

With this situation the effective lifetime (τ_{eff}) is evaluated by using this equation cited by different authors[44–46]:

$$\tau_{eff} = \frac{\int t * I(t) * dt}{\int I(t) * dt}$$

If there are energy transfer processes:

$$\frac{1}{\tau_{eff}} = \frac{1}{\tau_0} + W_{ET}$$

W_{ET} represents the energy transfer probability and τ_0 is the intrinsic lifetime which can be measured if the concentration of active ions is low enough to neglect the interaction between ions, and therefore the energy transfer probabilities.

In the case of Nd^{3+} doped perovskites (see figure 10) the relaxation observed was the $^4S_{3/2} \rightarrow {}^4I_{9/2}$, exciting wavelength was set at 690 nm and the emission was observed at 934 nm wavelength. The decay presents the same behaviour as the Er^{3+} doped perovskites.

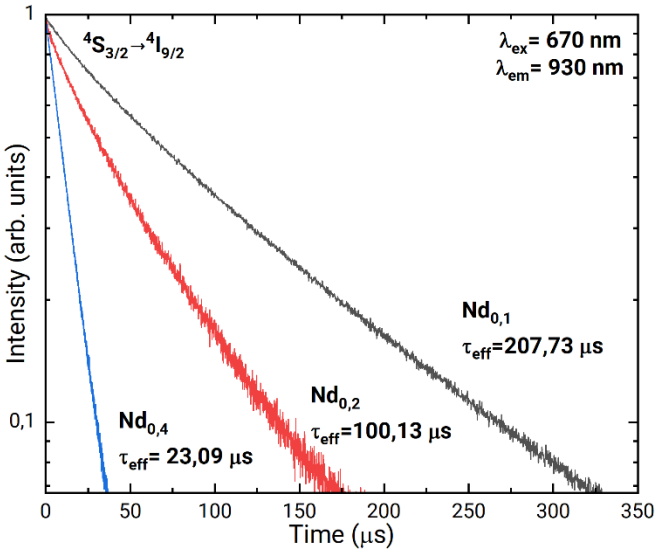

Figure 10. Luminescence decay curves of NIR emissions of different Nd3+ doped perovskites.

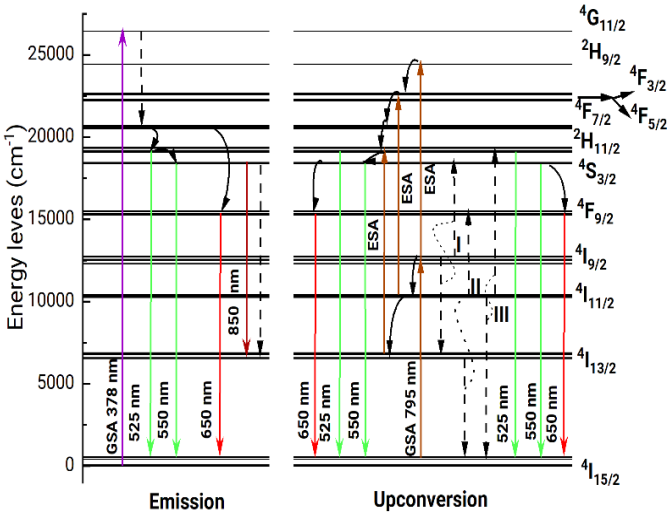

Figure 11. Partial energy diagram of Er^{3+} ions showing: At left different radiative transitions (downward solid lines) after the $^4I_{15/2}\rightarrow{}^4G_{11/2}$ ground state absorption (GSA) by excitation with a laser at 378 nm. Multiphonon (black solid lines) and energy transfer(dashed lines). At the right the upconverted emissions under a 790 nm laser excitation, excited states absorption (ESA, as upward solid lines) and energy transfer upconversion (Roman numbers), non-radiative processes are also shown as dashed downward lines.

The variation of the lifetime of the $^4I_{13/2}$ level with the concentration of Er^{3+} can be explained with the existence of a resonant cross-relaxation channel ($^4I_{13/2}$, $^4I_{13/2}\rightarrow{}^4I_{15/2}$, $^4I_{9/2}$), or with energy transfer from Er^{3+} ions to quenching traps[44].

Taking as intrinsic lifetime (τ_0) the time measured for the sample with the lowest lanthanide concentration in which energy transfer processes are considered not to occur. It is estimated that the energy transfer probability Ln^{3+}-Ln^{3+} (W_{ET}) for the samples with higher concentration, obtained from equation 2 are, for $Er_{0,4}$ sample the value of energy transfer is estimated in W_{ET}= 143811 s^{-1} which is a really huge value, indicating that energy transfer probability is important in the quenching of these luminescence due to the competition between two processes, the spontaneous radiative deexcitation and cross relaxation in the $^4I_{13/2}$ level. The values of energy transfer probabilities for the Neodymium are estimated for the $Nd_{0,2}$ in W_{ET}=5173,1 s^{-1} and for the highest concentration $Nd_{0,4}$ in W_{ET}=38495 s^{-1}. This value indicates that the energy transfer probabilities become significant when the concentration of neodymium is higher than 0,2.

3.2.2 Upconversion processes

Some of the Erbium bands are susceptible to develop the up-conversion (UC) phenomenon, this process as explained in the introduction involves one metastable state, looking at the absorption spectra(see figure 6) we decide to excite the Er^{3+} at 795 nm (NIR) which corresponds with the $^4I_{15/2}\rightarrow{}^4I_{9/2}$ transition, this energy will be transmitted to higher energy levels such us $^4S_{3/2}$ or $^4F_{9/2}$ (Vis) and emitted as upconverted emission light. The intensity of UC emission can be studied as a function of the pump power, studying the intensity of the signal at different pump power will follow the following equation:

$$I = K * P^n$$

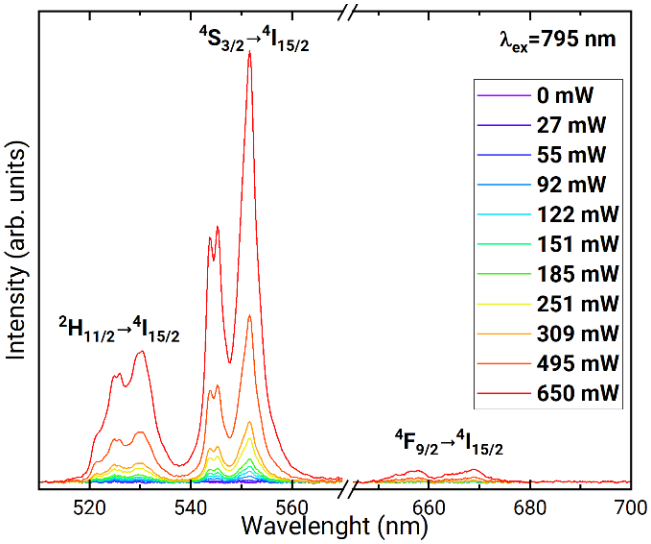

Figure 12. Upconverted emission spectra of the $Er_{0,05}Sr_{0,95}MoO_3$ Perovskite, the two principals Er^{3+} upconversion emissions are marked.

where *K* is a constant and *n* indicates de number of photons involved in the UC process, When the logarithmic UC emission intensity is represented as a function of logarithmic pump power, this leads to a straight line with a slope, indicating the value of n, If

the value is more than ~1,5 it indicates that 2 photons are involved in this process. The discrepancy of the obtained value and the value of photons involved (n=2) is explained by the saturation of the UC process when the power increases, causing the slope of the fitting to decrease[47].

Figure 12 indicates a direct relation between the signal intensity and the pump power, if we focus on just one peak and study its logarithm increase vs the logarithmic increase of the laser power, we can obtain the mentioned straight lines as shown in figure 12.

Figure 13 shows that a decrease in the concentration of Er^{3+} leads to higher values of *n*, this proves a dependence between Er^{3+} concentration and luminescence. The enhancement on the upconverted emissions is explained by different cross-relaxation processes as explained for the figure 11.

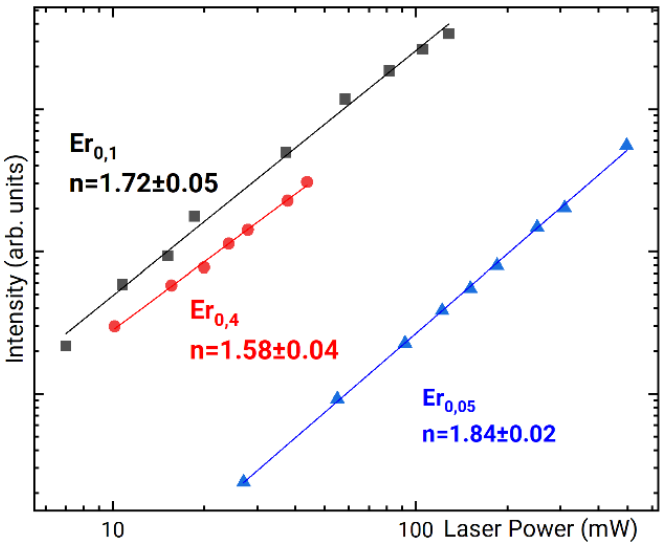

Figure 13. Upconversion intensity vs laser pump of different erbium perovskites.

4 Conclusions

The Er^{3+}/Nd^{3+} doped $SrMoO_3$ perovskites has been successfully synthetized by ceramic method in a range of concentrations. X-Ray diffraction confirm that the compounds obtained are perovskites with tetragonal symmetry and with the space group $I_{41/a}$ (nº 88), with Scanning electron microscopy the shape of the nanocrystalline powder is determined as agglomerated flakes and an approximation of the size is stablish in 10 - 20 µm. The optical characterization of the perovskites was done where the peaks observed in the absorption and luminescence spectra are due the incorporation of Er^{3+}/Nd^{3+} in the structure. Different luminescence decay dynamics are observed for both lanthanides, indicating that they have some cross-relaxation channels mechanism. When the Er^{3+} doped perovskites are irradiated with 795nm laser excitation wavelength, they show an intense green upconverted luminescence. This makes these new perovskites a promising and interesting materials for optical devices.

Acknowledgements

I would like to thank both of my supervisors for having tutored this work , to professor Antonio Diego Lozano for always being willing to work with me and proposing new ideas and to professor Víctor Lavín for opening the doors of his laboratory and teaching me everything I know about luminescence and have tried to translate into this work, without them this work would not have been possible. I would also like to thank my co-worker, Fernando Déniz, for always being there, and for being a really important support during the development of this master's degree.

5 References

1. Assirey, E. A. R. Perovskite synthesis, properties, and their related biochemical and industrial application. *Saudi Pharmaceutical Journal* vol. 27 817–829 Preprint at https://doi.org/10.1016/j.jsps.2019.05.003 (2019).
2. Galasso, F. S. *Structure, Properties, and preparation of Perovskite-type compounds*. (Pergamon Press, 2013).
3. Dekker, M. *Properties, and applications of perovskites-type oxides*. (CRC Press).
4. Sun, C., Alonso, J. A. & Bian, J. Recent Advances in Perovskite-Type Oxides for Energy Conversion and Storage Applications. *Advanced Energy Materials* vol. 11 Preprint at https://doi.org/10.1002/aenm.202000459 (2021).
5. Liu, X., He, J. H., Sakthivel, R. & Chung, R. J. Rare earth erbium molybdate nanoflakes decorated functionalized carbon nanofibers: An affordable and potential catalytic platform for the electrooxidation of phenothiazine. *Electrochim Acta* **358**, (2020).
6. Rao, C. N. R. Perovskite oxides and high-temperature superconductivity. *Ferroelectrics* **102**, 297–308 (1990).
7. Rørvik, P. M., Grande, T. & Einarsrud, M. A. One-dimensional nanostructures of ferroelectric perovskites. *Advanced Materials* vol. 23 4007–4034 Preprint at https://doi.org/10.1002/adma.201004676 (2011).
8. Cascos, V., Fernández-Díaz, M. T. & Alonso, J. A. Al-Doped SrMoO3 Perovskites as Promising Anode Materials in Solid Oxide Fuel Cells. *Materials* **15**, (2022).
9. Cascos, V., Troncoso, L., Alonso, J. A. & Fernández-Díaz, M. T. Design of new Ga-doped SrMoO3 perovskites performing as anode

materials in SOFC. *Renew Energy* **111**, 476–483 (2017).
10. Cascos, V., Alonso, J. A. & Fernández-Díaz, M. T. Novel Mg-doped SrMoO3 Perovskites designed as anode materials for solid oxide fuel cells. *Materials* **9**, (2016).
11. Kachhap, S., Singh, S., Singh, A. K. & Singh, S. K. Lanthanide-doped inorganic halide perovskites (CsPbX3): Novel properties and emerging applications. *Journal of Materials Chemistry C* vol. 10 3647–3676 Preprint at https://doi.org/10.1039/d1tc05506b (2022).
12. Mir, W. J., Sheikh, T., Arfin, H., Xia, Z. & Nag, A. Lanthanide doping in metal halide perovskite nanocrystals: spectral shifting, quantum cutting and optoelectronic applications. *NPG Asia Materials* vol. 12 Preprint at https://doi.org/10.1038/s41427-019-0192-0 (2020).
13. Wang, J., Wang, F., Luo, Y., Li, X. & Jia, Y. Improved the stability and enhanced luminescence of Er doped CsPbBr3 perovskite. *Mater Sci Semicond Process* **151**, (2022).
14. S. F., L.-L. *et al.* Optical nanothermometer based on the calibration of Stokes and upconverted green emissions of Er(3+) ions in Y3Ga5O12 nano-garnets. *RSC Adv* **4**, (2014).
15. Hernández-Rodriguez, M. A. *et al.* Analysis of the upconversion emission of yttrium orthoaluminate nano-perovskite co-doped with Er3+/Yb3+ ions for thermal sensing applications. *J Lumin* **202**, 316–321 (2018).
16. Venkataiah, G. *et al.* Spectroscopic studies on Yb3+-doped tungsten-tellurite glasses for laser applications. *J Non Cryst Solids* **479**, 9–15 (2018).
17. Hernández-Rodríguez, M. A. *et al.* 1000 K optical ratiometric thermometer based on Er3+ luminescence in yttrium gallium garnet. *J Alloys Compd* **886**, (2021).
18. Stanley, A. T., Harris, E. A., Searle, T. M. & Parker, J. M. *Upconversion in neodymium doped fluoride glasses. Journal of Non-Crystalline Solids* vol. 161 (1993).
19. Som, T. & Karmakar, B. Efficient green and red fluorescence upconversion in erbium doped new low phonon antimony glasses. *Opt Mater (Amst)* **31**, 609–618 (2009).
20. Amorim, H. T. *et al. Energy upconversion luminescence in neodymium-doped tellurite glass. Journal of Alloys and Compounds* vol. 346 www.elsevier.com/locate/jallcom (2002).
21. Som, T. & Karmakar, B. Efficient green and red fluorescence upconversion in erbium doped new low phonon antimony glasses. *Opt Mater (Amst)* **31**, 609–618 (2009).
22. Auzel, F. Upconversion and Anti-Stokes Processes with f and d Ions in Solids. *Chemical Reviews* vol. 104 139–173 Preprint at https://doi.org/10.1021/cr020357g (2004).
23. Ustione, A. & Piston, D. W. A simple introduction to multiphoton microscopy. *J Microsc* **243**, 221–226 (2011).
24. So, P. T. C., Dong, C. Y., Masters, B. R. & Berland, K. M. *TWO-PHOTON EXCITATION FLUORESCENCE MICROSCOPY.* www.annualreviews.org (2000).
25. Lewenstein, M., Balcou, P., Ivanov, ′t Anne L′ huillier, M. Y., Corkum, P. B. & Livermore, L. *Theory of high-harmonic generation by low-frequency laser fields.* vol. 49 (1994).
26. Ghimire, S. & Reis, D. A. High-harmonic generation from solids. *Nature Physics* vol. 15 10–16 Preprint at https://doi.org/10.1038/s41567-018-0315-5 (2019).
27. Nadort, A., Zhao, J. & Goldys, E. M. Lanthanide upconversion luminescence at the nanoscale: Fundamentals and optical properties. *Nanoscale* vol. 8 13099–13130 Preprint at https://doi.org/10.1039/c5nr08477f (2016).
28. Wang, F. & Liu, X. Recent advances in the chemistry of lanthanide-doped upconversion nanocrystals. *Chem Soc Rev* **38**, 976–989 (2009).
29. Wenger, O. S., Gamelin, D. R. & Güdel, H. U. Chemical modification of transition metal upconversion properties: Exchange enhancement of Ni2+ upconversion rates in Ni2+:RbMnCl3 [12]. *Journal of the American Chemical Society* vol. 122 7408–7409 Preprint at https://doi.org/10.1021/ja000979o (2000).
30. Zhang, F. *Photon upconversion nanomaterials.* (Springer, 2015).
31. Chen, J. & Zhao, J. X. Upconversion nanomaterials: Synthesis, mechanism, and applications in sensing. *Sensors* vol. 12 2414–2435 Preprint at https://doi.org/10.3390/s120302414 (2012).
32. Suyver, J. F. *et al.* Novel materials doped with trivalent lanthanides and transition metal ions showing near infrared to visible photon upconversion. *Opt Mater (Amst)* **27**, 1111–1130 (2005).
33. Weiss, C. A. & Moser, R. D. *Sample Preparation of Nano-sized Inorganic Materials for Scanning Electron Microscopy or Transmission Electron Microscopy Scientific Operating Procedure SOP-P-2 Geotechnical and Structures Laboratory.* www.erdc.usace.army.mil. (2015).
34. Rietveld, H. M. A Profile Refinement Method for Nuclear and Magnetic Structures. *J. Appl. Cryst* **2**, 65 (1969).
35. Rodriguez-Carvajal, J. Recent advances in magnetic structure determination neutron powder diffraction. *Physica B* **192**, 113 (1993).
36. Rodríguez-Carvajal, J. & Roisnel, T. Line Broadening Analysis Using Fullprof: Determination of Microstructural Properties.

in *Materials Science Forum* vols 443–444 123–126 (Trans Tech Publications Ltd, 2004).
37. Macquart, R. B., Kennedy, B. J. & Avdeev, M. Neutron diffraction study of phase transitions in perovskite-type strontium molybdate SrMoO3. *J Solid State Chem* **183**, 250–255 (2010).
38. Reimer, L. Electron Scattering and Diffusion. in *Scanning Electron Microscopy* 57–134 (1998).
39. Cai, W., Fu, C., Gao, J. & Chen, H. Effects of grain size on domain structure and ferroelectric properties of barium zirconate titanate ceramics. *J Alloys Compd* **480**, 870–873 (2009).
40. Karmakar, B. & Dwivedi, R. N. FT-IRRS, UV-Vis-NIR absorption and green upconversion in Er3+ doped lead silicate glass. *J Non Cryst Solids* **342**, 132–139 (2004).
41. Rudenko, M. V. *et al.* Erbium upconversion luminescence from sol-gel derived multilayer porous inorganic perovskite films. *J Adv Dielectr* **12**, (2022).
42. Dieke, G. H. *Spectra and energy levels of rare earth ions in crystals*. (Wiley, 1968).
43. Di Bartolo, B. Energy Transfer among Ions in Solids. in 103–204 (1984). doi:10.1007/978-1-4613-2407-2_2.
44. Venkatramu, V. *et al.* Synthesis, structure, and luminescence of Er 3+-doped Y 3Ga 5O 12 nano-garnets. *J Mater Chem* **22**, 13788–13799 (2012).
45. Georgescu, S. *et al. Concentration effects on the up conversion from the 4I13,2 level of Er3+ in YAG. OPTICS COMMUNICATIONS* vol. 8 (1990).
46. Bergstrand, J. *et al.* On the decay time of upconversion luminescence. *Nanoscale* **11**, 4959–4969 (2019).
47. Pollnau, M., Gamelin, D. R., Lüthi, S. R., Güdel, H. U. & Hehlen, M. P. Power dependence of upconversion luminescence in lanthanide and transition-metal-ion systems. *Phys Rev B* **61**, 3337–3346 (2000).